BRIEF COMMUNICATION
PUBLISHED ONLINE: 26 SEPTEMBER 2016 | DOI: 10.1038/NCHEMBIO.2185
nature chemical biology

Thermal profiling reveals phenylalanine hydroxylase as an off-target of panobinostat

Isabelle Becher[1,2], Thilo Werner[1], Carola Doce[1], Esther A Zaal[3], Ina Tögel[1], Crystal A Khan[4], Anne Rueger[1], Marcel Muelbaier[1], Elsa Salzer[1], Celia R Berkers[3], Paul F Fitzpatrick[4], Marcus Bantscheff[1]* & Mikhail M Savitski[1,2]*

We describe a two-dimensional thermal proteome profiling strategy that can be combined with an orthogonal chemoproteomics approach to enable comprehensive target profiling of the marketed histone deacetylase inhibitor panobinostat. The *N*-hydroxycinnamide moiety is identified as critical for potent and tetrahydrobiopterin-competitive inhibition of phenylalanine hydroxylase leading to increases in phenylalanine and decreases in tyrosine levels. These findings provide a rationale for adverse clinical observations and suggest repurposing of the drug for treatment of tyrosinemia.

In drug discovery, comprehensive target identification is a key challenge for rationalizing a drug's therapeutic and adverse effects[1]. A recently introduced proteomics technology termed thermal proteome profiling (TPP) uses the cellular thermal shift assay[2] and multiplexed quantitative MS to enable unbiased identification of drug targets in living cells[2–5].

Here we combine TPP and affinity enrichment–based chemoproteomics[6–8] to identify the protein targets of the marketed histone deacetylase (HDAC) inhibitor panobinostat[9] (1) (Farydak, **Supplementary Results**, **Supplementary Fig. 1**). Panobinostat has been approved by the US Food and Drug Administration for treatment of multiple myeloma[10] and is currently in clinical trials for other malignant diseases. Some side effects associated with panobinostat treatment[11], such as hypothyroidism, seizures and tremors, have not been observed with other hydroxamate-based HDAC inhibitors, suggesting undescribed off-target activities (**Supplementary Table 1**).

To comprehensively detect dose-dependent effects of small-molecule inhibitors on their targets with TPP, we devised a two-dimensional strategy (2D-TPP) (**Supplementary Fig. 1**) that measures proteome-wide protein stability at 12 temperatures and 5 different compound concentrations in 6 multiplexed liquid chromatography–tandem MS (LC-MS/MS) analyses using tandem mass tags (TMT10)[12]. For the majority of proteins, this method enables sensitive detection of dose-dependent stabilization or destabilization close to their melting point (T_m).

To differentiate between direct targets of panobinostat and indirect effects, we performed 2D-TPP in HepG2 human liver cancer cells and cell extracts[13], identifying and quantifying 6,438 and 5,203 proteins, respectively (**Supplementary Data Sets 1** and **2** and **Supplementary Fig. 2**). In the cells, 23 proteins showed concentration-dependent changes in thermal stability, whereas 5 showed such changes in cell extracts. Four proteins were dose-dependently stabilized in both the cellular and cell extract experiments, indicating that these proteins were direct targets of panobinostat (**Fig. 1a**, **Supplementary Figs. 3** and **4** and **Supplementary Tables 2** and **3**). When cells were heated to 50 °C, close to the melting points of the primary panobinostat targets HDAC1 and HDAC2 (**Supplementary Data Set 3**), half-maximal stabilization was observed at 20 nM. At temperatures substantially above the melting point, higher compound concentrations were required for maximal stabilization (**Fig. 1a** and **Supplementary Fig. 4**). Absolute and relative potencies determined at temperatures close to the melting points of HDAC1, HDAC2, HDAC6 and HDAC10 isoforms were in close agreement with a recent report measuring target engagement with recombinant constructs[14].

Some proteins had altered abundances at all temperatures, suggesting a change in expression or extractability rather than in thermal stability. Increases in abundance of histones H4 and H2A (**Fig. 1a** and **Supplementary Fig. 5**) in panobinostat-treated samples can be explained as histone hyperacetylation caused by HDAC inhibition. Consequently, in the euchromatin state, DNA is wrapped less tightly around the histones, making them more readily extractable.

Aside from known HDAC targets, two other proteins—tetratricopeptide repeat domain 38 (TTC38) and phenylalanine hydroxylase (PAH)—showed increased thermal stability at low panobinostat concentrations, with $-\log_{10}$ half-maximal effective concentration (pEC_{50}) values of 8.1 and 7.2, respectively, at the temperatures closest to the proteins' melting points in the cellular experiment (**Supplementary Fig. 4**, **Supplementary Table 2** and **Supplementary Data Set 3**). Little is known about TTC38. A homolog of TTC38 in *Streptomyces toyocaensis* has been postulated to hydroxylate tyrosine at the β-carbon in biosynthesis of the glycopeptide antibiotic A47934 (ref. 15). Panobinostat was found to affect the thermal stability of TTC38 in cellular TPP experiments[13], but whether TTC38 is a direct or indirect target of the drug remained unclear. We found stabilization of TTC38 in cell extracts and did not observe other specifically enriched panobinostat targets in coimmunoprecipitations (**Supplementary Fig. 6** and **Supplementary Data Set 4**), suggesting that TTC38 is a direct target of panobinostat. PAH has not been identified as a panobinostat target in previous TPP work[4,13].

TTC38 and PAH were not stabilized in dose-dependent TPP experiments with the structurally distinct marketed HDAC inhibitor vorinostat (2), indicating that the hydroxamate warhead alone is not sufficient for potently binding these proteins (**Supplementary Fig. 7** and **Supplementary Data Set 5**). Panobinostat also had a dose-dependent effect on the stability of the transmembrane proteins fatty acid desaturase (FADS1) and FADS2, which regulate desaturation of fatty acids (**Fig. 1a**). These proteins were identified only in the cellular TPP experiment, where the

[1]Cellzome GmbH, Heidelberg, Germany. [2]Genome Biology Unit, European Molecular Biology Laboratory, Heidelberg, Germany. [3]Biomolecular Mass Spectrometry and Proteomics, Utrecht University, Utrecht, the Netherlands. [4]Department of Biochemistry, University of Texas Health Science Center, San Antonio, Texas, USA. *e-mail: marcus.x.bantscheff@gsk.com or mikhail.savitski@embl.de

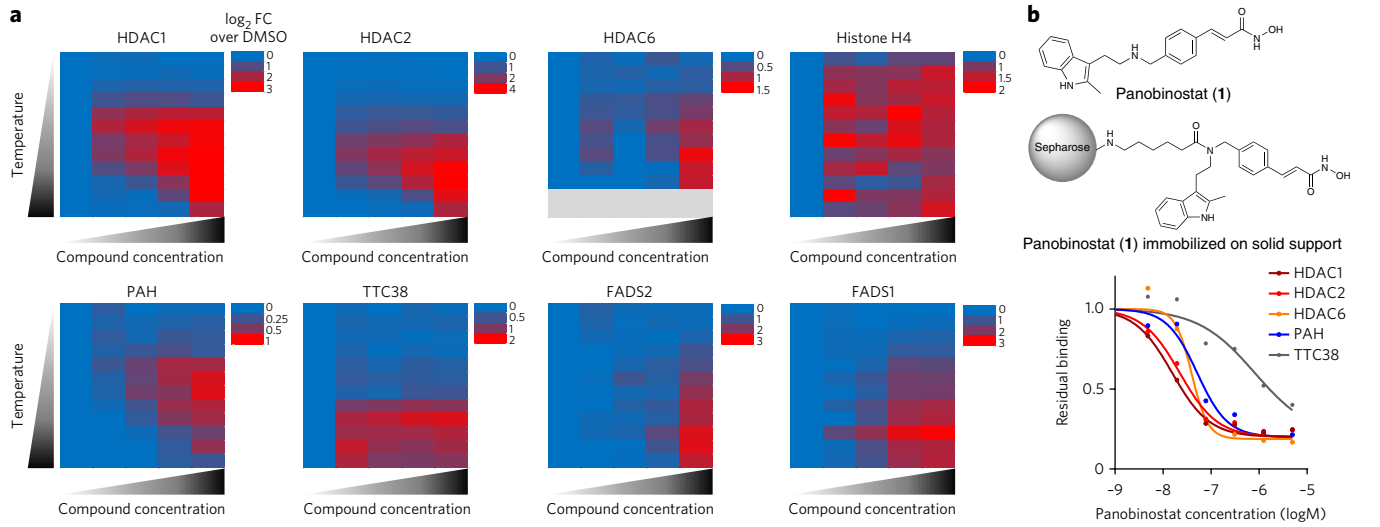

Figure 1 | Proteins showing changes in thermal stability in 2D-TPP experiments and analyzed in the chemoproteomics experiment with panobinostat. (**a**) Heat maps showing change in protein abundance for panobinostat at different concentrations (5, 1, 0.143 and 0.02 μM), calculated with respect to DMSO (negative control, left column in each plot) in a cell-based 2D-TPP experiment. Temperatures applied were 42, 44.1, 46.2, 48.1, 50.4, 51.9, 54.0, 56.1, 58.2, 60.1, 62.4 and 63.9 °C. FC, fold change. (**b**) Top, structures of panobinostat and panobinostat immobilized on beads. Bottom, dose-response curves for proteins in cell extracts after incubation with panobinostat and addition of panobinostat immobilized on beads for competition. Data represent average of 2 biological replicates (Online Methods).

mild detergent NP-40 was used for cell extraction, thus enabling thermal profiling of transmembrane proteins[16].

Notably, the 2D-TPP strategy enabled more sensitive identification of panobinostat targets than previously published methods (**Supplementary Data Set 6** and **Supplementary Fig. 8**).

We proceeded with panobinostat target profiling using an orthogonal affinity enrichment–based chemoproteomics approach. In a previous dose-dependent competitive binding study with cell extracts using a vorinostat analog immobilized on Sepharose beads[17], TTC38 and PAH were not identified as targets of panobinostat. As vorinostat did not affect these proteins in TPP experiments, we reasoned that immobilizing panobinostat should provide a more suitable capturing matrix for these proteins (**Fig. 1b** and **Supplementary Fig. 9**). Capturing and competitive binding of TTC38 and PAH in these experiments strongly depended on buffer compositions (**Supplementary Data Set 7** and **Supplementary Table 4**) and was completely abrogated in the presence of detergents.

Under detergent-free conditions, TTC38 and PAH were bound by panobinostat with apparent pK_d (pK_d^{app}) values of 6.1 and 7.3, respectively (**Fig. 1b**, **Supplementary Fig. 10**, **Supplementary Data Set 7** and **Supplementary Tables 2** and **4**). Panobinostat affinities for HDAC1 and HDAC2 agreed well with the pEC_{50} values measured by 2D-TPP in the cell-extract and cell-based experiments at the temperatures closest to the melting points (**Supplementary Table 2**), confirming that compound-dependent target stabilization determined at temperatures close to the melting point is a good measure for target potency in 2D-TPP experiments.

Loss-of-function mutations in the PAH gene lead to impaired phenylalanine metabolism and cause phenylketonuria, a monogenic disease leading to severe developmental deficiencies. Even mildly (3- to 5-fold) increased phenylalanine levels in plasma can cause cognitive deficits[18]. PAH inhibition can also lead to decreased tyrosine levels, which can cause symptoms mimicking hypothyroidism[19], a common panobinostat side effect[20]. To investigate whether

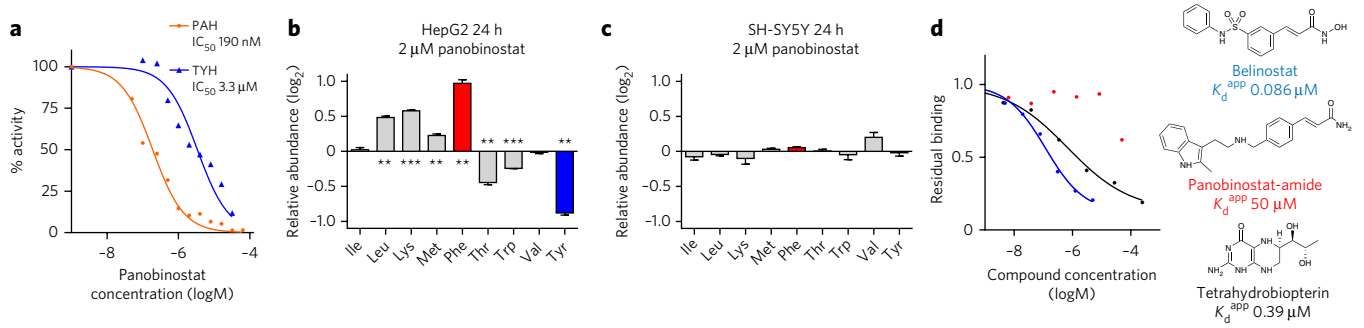

Figure 2 | Panobinostat inhibits PAH activity in a tetrahydrobiopterin-competitive manner and requires the *N*-hydroxycinnamide moiety. (**a**) Enzymatic assay data showing inhibition of PAH and tyrosine hydroxylase (TYH) activity by panobinostat. For PAH inhibition, data represent the average of 2 replicates. For TYH inhibition, data represent a single experiment. (**b**,**c**) Log_2 ratios of intracellular levels of eight essential amino acids and tyrosine between panobinostat and vehicle treatment after 24 h in HepG2 (**b**) or SH-SY5Y (**c**) cells. Data are mean ± s.e.m. from 3 biological replicates. $^{**}P < 0.01$, $^{***}P < 0.001$ for deviation of the observed ratio from 0 (*t*-test). Essential amino acids were used for normalization (Online Methods). (**d**) Left, dose-response curves for PAH in cell extracts incubated with belinostat (blue), panobinostat-amide (red) or tetrahydrobiopterin (black) at different concentrations after addition of bead-immobilized panobinostat. Data represent the average of 2 replicates measured in 2 biological replicates (Online Methods). Right, structures of belinostat, panobinostat-amide and tetrahydrobiopterin.

binding of panobinostat causes PAH inhibition, we performed enzymatic assays with PAH purified from rat liver. Panobinostat inhibited tyrosine synthesis with a half-maximal inhibitory concentration (IC_{50}) value of 190 nM when the active enzyme was first incubated with the inhibitor for 5 min (**Fig. 2a**, **Supplementary Fig. 11** and **Supplementary Table 5**), indicating time-dependent inhibition. Panobinostat did not affect activation of the enzyme by phenylalanine, suggesting binding to the active site rather than the allosteric phenylalanine-binding site. Tyrosine hydroxylase, which has a catalytic site very similar to that of PAH, yielded only weak inhibition (IC_{50} 3.3 µM) (**Fig. 2a**). Next, we investigated whether PAH inhibition by panobinostat alters cellular phenylalanine levels. In contrast to SH-SY5Y cells, which do not express PAH[21] (**Supplementary Data Set 8** and **Supplementary Fig. 12**), HepG2 cells showed significantly higher intracellular phenylalanine levels after incubation with 2 µM panobinostat (**Fig. 2b**,**c**, **Supplementary Fig. 13** and **Supplementary Data Sets 9** and **10**). Increased phenylalanine levels were also observed in the medium of HepG2 cells but not of SH-SY5Y cells, suggesting reduced phenylalanine uptake upon PAH inhibition (**Supplementary Figs. 14** and **15**).

To investigate the mechanism by which panobinostat inhibits PAH, we performed additional pulldown experiments with the panobinostat matrix. When the phenylanine analog p-chlorophenylalanine (**3**) was spiked into cell extracts at concentrations higher than 1.25 mM, more PAH was captured on the beads, consistent with the idea that the overall fraction of activated enzyme increased and was captured by immobilized panobinostat through binding to the active site (**Supplementary Fig. 16** and **Supplementary Table 6**). The PAH cofactor tetrahydrobiopterin (**4**), which binds to the active site, showed dose-dependent competitive binding to PAH ($pK_d^{app} = 6.41$) (**Fig. 2d** and **Supplementary Data Set 11**) but did not affect matrix binding of the other panobinostat targets. We hypothesized that chelation of Fe(II) in the catalytic domain of PAH by the hydroxamic acid group of panobinostat could contribute to active site binding. In line with this assumption, panobinostat-amide (**5**), in which the *N*-hydroxycinnamide moiety of panobinostat is replaced by a cinnamide, was inactive in the beads-based competition-binding assay (**Fig. 2d** and **Supplementary Data Set 12**). To further explore the structure affinity relationship of PAH inhibition, we compared chemoproteomics profiles of panobinostat with experiments performed using the marketed HDAC inhibitor belinostat (**6**) as a competitor. Both inhibitors have the *N*-hydroxycinnamide warhead for chelation of Zn^{2+} in the active site of HDACs, but they are otherwise structurally distinct. Belinostat inhibited PAH binding to panobinostat beads ($K_d^{app} = 0.086$ µM), demonstrating that *N*-hydroxycinnamides are potent PAH inhibitors (**Fig. 2d**). Potent off-target binding was also observed for the oncoprotein lactoylglutathione lyase GLO1 (ref. 22) and for glucosamine-6-phosphate deaminase 1 (**Supplementary Table 2**, **Supplementary Fig. 17** and **Supplementary Data Set 13**).

Taken together, these results provide evidence for potent binding of panobinostat to the active site of PAH via its *N*-hydroxycinnamide moiety, which leads to increases in cellular phenylalanine and decreases in tyrosine levels. Tyrosine is essential for biosynthesis of thyroid hormones; thus, inhibition of PAH provides a rationale for the reduced thyroid hormone levels observed in hypothyroid animals. Given these findings, we suggest that it would be advisable to monitor phenylalanine and tyrosine levels in patients taking panobinostat who show symptoms of hypothyroidism and when the drug is administered to young children. Selective inhibitors of PAH might provide therapeutic opportunities for treatment of type 1 tyrosinemia—an orphan disease caused by inborn deficiency of fumarylacetoacetate hydrolase, an enzyme in the tyrosine catabolic pathway. Diet supplementation with phenylalanine in conjunction with PAH inhibition could reduce hypophenylalaninemia and mitigate impaired neurocognitive development[23].

In general, given the unexpected and high-potency off-targets identified for panobinostat and belinostat in this work, study of only the known HDAC targets may not be sufficient to explain the pleiotropic effects of HDAC inhibitors in different cellular and *in vivo* settings.

Received 15 January 2016; accepted 20 July 2016;
published online 26 September 2016

Methods

Methods and any associated references are available in the online version of the paper.

Accession codes. ProteomicsDB: MS data have been deposited under accession code PRDB004255.

References

1. Simon, G.M., Niphakis, M.J. & Cravatt, B.F. *Nat. Chem. Biol.* **9**, 200–205 (2013).
2. Martinez Molina, D. *et al. Science* **341**, 84–87 (2013).
3. Martinez Molina, D. & Nordlund, P. *Annu. Rev. Pharmacol. Toxicol.* **56**, 141–161 (2016).
4. Savitski, M.M. *et al. Science* **346**, 1255784 (2014).
5. Huber, K.V. *et al. Nat. Methods* **12**, 1055–1057 (2015).
6. Bantscheff, M. & Drewes, G. *Bioorg. Med. Chem.* **20**, 1973–1978 (2012).
7. Schenone, M., Dančík, V., Wagner, B.K. & Clemons, P.A. *Nat. Chem. Biol.* **9**, 232–240 (2013).
8. Ziegler, S., Pries, V., Hedberg, C. & Waldmann, H. *Angew. Chem. Int. Edn Engl.* **52**, 2744–2792 (2013).
9. Atadja, P. *Cancer Lett.* **280**, 233–241 (2009).
10. Bailey, H., Stenehjem, D.D. & Sharma, S. *J. Blood Med.* **6**, 269–276 (2015).
11. Younes, A. *et al. J. Clin. Oncol.* **30**, 2197–2203 (2012).
12. Werner, T. *et al. Anal. Chem.* **84**, 7188–7194 (2012).
13. Franken, H. *et al. Nat. Protoc.* **10**, 1567–1593 (2015).
14. Robers, M.B. *et al. Nat. Commun.* **6**, 10091 (2015).
15. Pootoolal, J. *et al. Proc. Natl. Acad. Sci. USA* **99**, 8962–8967 (2002).
16. Reinhard, F.B. *et al. Nat. Methods* **12**, 1129–1131 (2015).
17. Bantscheff, M. *et al. Nat. Biotechnol.* **29**, 255–265 (2011).
18. Diamond, A. *Acta Paediatr. Suppl.* **407**, 89–91 (1994).
19. Degroot, L.J. & Niepomniszcze, H. *Metabolism* **26**, 665–718 (1977).
20. Novartis. Farydak prescribing information, revised 02/2016. (2016).
21. Uhlén, M. *et al. Mol. Cell. Proteomics* **4**, 1920–1932 (2005).
22. Hosoda, F. *et al. Oncogene* **34**, 1196–1206 (2015).
23. van Vliet, D. *et al. JIMD Rep.* **18**, 117–124 (2015).

Acknowledgments

We thank J. Stuhlfauth for cell culture; M. Jundt, K. Kammerer, M. Klös-Hudak, M. Paulmann and T. Rudi for expert technical assistance; and G. Drewes for helpful suggestions. We also thank W.F. Mueller for providing cells for metabolomics experiments. P.F.F. acknowledges support from the Welch Foundation (grant AQ-1245). C.R.B. was supported by a VENI grant (project 722.013.009) from the Netherlands Organization for Scientific Research.

Author contributions

I.B., M.B. and M.M.S. conceived the project; I.B., T.W., M.B. and M.M.S. designed the biochemical, cell biological and MS experiments; I.B. and T.W. performed MS experiments; E.A.Z. and C.R.B. designed and performed metabolomics experiments; A.R. and M.M. synthesized the panobinostat-amide and gave advice; P.F.F. and C.A.K. designed and performed enzyme activity experiments; I.B., I.T. and E.S. performed biochemical and cell biological experiments; I.B., T.W., C.D., M.B. and M.M.S. contributed to data analysis; E.A.Z., C.R.B. and P.F.F. contributed to the manuscript; I.B., M.B. and M.M.S. wrote the manuscript.

Competing financial interests

The authors declare competing financial interests: details are available in the online version of the paper.

Additional information

Any supplementary information, chemical compound information and source data are available in the online version of the paper. Reprints and permissions information is available online at http://www.nature.com/reprints/index.html. Correspondence and requests for materials should be addressed to M.B. or M.M.S.

ONLINE METHODS

Reagents and cell culture. Reagents and medium were purchased from Sigma-Aldrich unless otherwise noted. PBS was prepared using 137 mM NaCl, 2.7 mM KCl, 10 mM Na_2HPO_4 and 2 mM KH_2PO_4 at pH 7.4 and supplemented with one tablet of EDTA-free protease inhibitors (Roche Diagnostics) per 25 ml. HepG2 cells were grown in MEM containing 10% FCS supplemented with 1 mM sodium pyruvate and 1% nonessential amino acids at a maximum of 80% confluence. SH-SY5Y cells were grown in DMEM/F-12 containing GlutaMAX and 10% FCS. Cells were harvested and centrifuged at 340 × *g* for 2 min at 4 °C and resuspended in 50 ml PBS. After a second wash step, the cells were resuspended in 10 ml ice-cold PBS and centrifuged again at 340 × *g* for 2 min at 4 °C. Washed pellets were either used directly or snap frozen in liquid nitrogen and stored at −80 °C until lysis. Both cell lines were checked for mycoplasma contamination and authenticated using the Promega kit MycoAlert.

Compound synthesis and characterization. Commercial compounds were obtained from Selleckchem, Santa Cruz Biotechnology, Sigma-Aldrich and Tocris. Panobinostat-amide was synthesized. Detailed information, including catalog numbers, for commercial compounds and analytical data are provided in the **Supplementary Note**.

2D-TPP experiments. *In cells.* Experiments were performed as described[16]. DMSO (vehicle) or panobinostat dissolved in DMSO at final concentrations of 5 µM, 1 µM, 0.143 µM or 0.02 µM was added to HepG2 cells (two plates for each concentration) and incubated for 90 min at 37 °C and 5% CO_2. All following steps were done as described[16] for the TPP temperature range (TR) experiment; the heat treatment was done with the following temperature range: 42.0–63.9 °C.

In cell extracts. Experiments were performed as described[16]. Cells were resuspended in ice-cold PBS. Following resuspension, cells were dounce homogenized with 20 strokes before ultracentrifugation (20 min at 4 °C and 100,000 × *g*). Protein concentration was determined by Bradford assay (BioRad). 800 µl lysate (concentration 2 mg/ml) was distributed to 5 tubes and incubated with vehicle (DMSO) or panobinostat (5 µM, 1 µM, 0.143 µM or 0.02 µM) for 15 min at 25 °C, then 100 µl per well of each reaction was transferred to a 96-well PCR plate. Samples were heated in parallel for 3 min to the target temperature (range: 42.0–60.1 °C) then incubated for 3 min at room temperature. After centrifugation (100,000 × *g*, 20 min, 4 °C) 80 µl of supernatant was subjected to gel electrophoresis and sample preparation for MS analysis.

HepG2 TPP TR. DMSO (vehicle) was added to HepG2 cells (one plate for each replicate) and incubated for 90 min at 37 °C and 5% CO_2, harvested by trypsinization and transferred to 50-ml conical centrifuge tubes. Cells were resuspended in PBS supplemented with vehicle and centrifuged for 5 min at 300 × *g*. This step was repeated once and the cells were resuspended in 1.5 ml PBS, resulting in a final concentration of 10^7 cells/ml. 100 µl per well of the suspension was transferred to 96-well PCR plates. Following a centrifugation step at 325 × *g* for 2 min at 4 °C, 80 µl of the supernatant was removed. The cells were resuspended and heated in a PCR block for 3 min to the desired temperature (37.0–66.3 °C) then incubated for 3 min at room temperature. 30 µl ice-cold PBS supplemented with 0.67% NP-40 and protease inhibitors was added to the samples. Cells were snap frozen in liquid nitrogen for 1 min, briefly thawed in a metal block at 25 °C, placed on ice and resuspended by pipetting. This freeze–thaw cycle was repeated once, followed by incubation with benzonase for 1 h at 4 °C. Samples were then centrifuged at 100,000 × *g* for 20 min at 4 °C. After centrifugation, 30 µl supernatant was transferred into a new tube. The supernatant was subjected to gel electrophoresis and sample preparation for MS analysis.

TPP TR profile ± 5 µM panobinostat. DMSO (vehicle) or 5 µM panobinostat was added to HepG2 cells and incubated for 90 min at 37 °C and 5% CO_2. All other procedures were as described above, but cells were not snap frozen before benzonase incubation.

TPP compound-concentration range (CCR) experiment using vorinostat. Experiments were performed as described[13]. Cells were treated with nine different vorinostat concentrations and vehicle control (DMSO) for 90 min at 37 °C, 5% CO_2. The following procedures were as described above; heat treatment was done at 56 °C for all samples.

Immunoprecipitation of TTC38. The enrichment of TTC38 was performed as described[24]. HepG2 cell extract (1 mg) was incubated with immobilized TTC38-specific antibody (10 µg, mouse, Abnova H00055020-B01P) as well as IgG control antibody (10 µg, Sigma-Aldrich, I8765). After 2 h incubation, beads were washed and enriched proteins eluted with 2× LDS sample buffer and subjected to gel electrophoresis and sample preparation for MS analysis.

Affinity-matrix based experiments. *Cell extract preparation.* Fresh or thawed cell pellets were resuspended in PBS supplemented with protease inhibitors, 1 mM $MgCl_2$ and benzonase (250 U/ml) and incubated for 1 h at 4 °C. Alternatively, cells were lysed in lysis buffer (50 mM Tris, pH 7.4, 5% glycerol, 1.5 mM MgCl2, 150 mM NaCl, 25 mM NaF, 1 mM Na_3VO_4) supplemented with 1% Nonidet P-40, protease inhibitors and benzonase (250 U/ml) and incubated for 1h at 4 °C. Lysates were centrifuged for 10 min at 20,000 × *g* at 4 °C, followed by ultracentrifugation for 1 h at 100,000 × *g* (4 °C). Protein concentration was determined by Bradford assay (Bio-Rad).

Determination of K_d^{app}. Experiments were performed as described[25], with minor changes. The panobinostat-derived solid support was prepared analogously to the procedure described[17,26]. Briefly, panobinostat was immobilized on NHS-activated Sepharose 4 Fast Flow beads (GE Healthcare) at a final concentration of 1 mM in DMSO, and the completion of the coupling reaction was monitored by HPLC. Remaining *N*-hydroxysuccinimide groups on the matrix were blocked with ethanolamine, and the beads were washed with DMSO and isopropanol (twice each). Briefly, 0.25 mg cell extract (with 0.4% NP-40 or without detergent) was incubated with six concentrations of panobinostat (dilution series) for 45 min at 4 °C. Beads were equilibrated in lysis buffer, and 1.75 µl beads were incubated with cell extract for 1 h at 4 °C then washed with lysis buffer. Bound proteins were eluted in LDS sample buffer supplemented with DTT before MS analysis samples were alkylated using iodoacetamide.

MS sample preparation and LC-MS/MS analysis. Gel lanes were cut into three slices covering the entire separation range (~2 cm) and subjected to in-gel digestion with either LysC (Wako Chemicals) for 2 h and trypsin (Promega) overnight or trypsin only for 4 h. Peptide samples were labeled with TMT10 (Thermo Fisher Scientific) reagents. The labeling reaction was performed in 40 mM triethylammonium bicarbonate, pH 8.53, at 22 °C and quenched with glycine. Labeled peptide extracts were combined, and samples from 2D-TPP, TPP CCR and TPP TR experiments were subjected to additional fractionation on an UltiMate 3000 (Dionex) by reversed-phase chromatography at pH 12 on a 1-mm Xbridge column (Waters), and 24 or 34 fractions were collected. Depending on the analytical depth required, 8–17 fractions were analyzed by LC-MS. Samples were vacuum dried and resuspended in 0.05% TFA. 50% of the sample was injected in an UltiMate 3000 nanoRLSC (Dionex) coupled to a Q Exactive Orbitrap Mass Spectrometer operated with Tune 2.3 and Xcalibur 3.0.63 (Thermo Fisher Scientific). Peptides were trapped on a 5 mm × 300 µm C18 column (Pepmap100, 5 µm, 300 Å, Thermo Fisher Scientific) in 0.05% TFA at 60 °C. Separation was performed on custom 50 cm × 100 µM (ID) reversed-phase columns (Reprosil) at 55 °C. Gradient elution was performed from 2% acetonitrile to 40% acetonitrile in 0.1% formic acid and 3.5% DMSO over 2 h. Mass spectrometers were operated with online injection and a data-dependent top-10 acquisition protocol 24 using 70,000 resolution and an ion target set to 3×10^6. Higher energy collision dissociation (HCD) scans were performed with 35% NCE at 35,000 resolution at m/z 200 with an ion target setting of 2×10^5 to avoid coalescence.

Peptide and protein identification and quantification. Mascot 2.4 (Matrix Science) was used for protein identification, and a 10-p.p.m. mass tolerance for peptide precursors and 20-mDa (HCD) mass tolerance for fragment ions was selected. Carbamidomethylation of cysteine residues and TMT modification of lysine residues were selected as fixed modifications, and methionine oxidation, N-terminal acetylation of proteins and TMT modification of peptide N termini were selected as variable modifications. The search database consisted

of a customized version of the International Protein Index database combined with a decoy version of the database created using a script supplied by Matrix Science. The following criteria for protein identifications were used: (i) for single spectrum-to-sequence assignments, we required this assignment to be the best match with a minimum Mascot score of 31 and a 10× difference over the next best assignment (using these criteria, the decoy search results indicated a <1% false discovery rate (FDR)); (ii) for multiple spectrum-to-sequence assignments and using the same parameters, the decoy search results indicate <0.1% FDR. Reporter ion intensities were extracted from the raw data and multiplied by ion accumulation times (measured in ms) to yield ion area, a measure proportional to the number of ions. Peptide spectrum matches were filtered according to the following criteria: mascot ion score >15, signal-to-background of the precursor ion >4, and signal-to-interference >0.5 (ref. 27). Fold changes were corrected for isotope purity as described and adjusted for interference caused by coeluting nearly isobaric peaks as estimated by the signal-to-interference measure[28]. Protein quantification values were calculated from individual spectra matching to unique peptides using a sum-based bootstrap algorithm; 95% confidence intervals were calculated for all protein fold changes that were quantified with >3 spectra. UniProt transmembrane domain annotation was used to classify proteins as membrane proteins by mapping the UniProt IDs on the IPI IDs.

Analysis of TPP TR experiments. TPP TR experiments were normalized and fitted with the following equation, as previously described[4]:

$$f(T) = \frac{1 - \text{plateau}}{1 + e^{-((a/T)-b)}} + \text{plateau}$$

where T is the temperature and a, b and 'plateau' are constants. The value of $f(T)$ at the lowest temperature T_{min} was set to 1. The melting point of a protein was defined as the temperature T_m at which half of the protein amount has been denatured, i.e.,

$$f(T_m) = 0.5$$

for proteins whose curves met the following three requirements: (i) fitted curves for both vehicle and compound-treated conditions had an R^2 of >0.8, (ii) the vehicle curve had a plateau of <0.3 and (iii) in each biological replicate, the steepest slope of the protein melting curve in the paired set of vehicle- and compound-treated conditions was below −0.06. In the visualization of data in **Supplementary Figure 8**, we additionally required that the melting points measured in both vehicle replicates differed by <1.5 °C for the same protein. To select proteins with significantly changed thermal stability after treatment in two biological replicates (two pairs of vehicle- and compound-treated experiments), we used the following, previously described[4], rules.

1. The melting point difference between vehicle- and compound-treated conditions for a protein had a Benjamini–Hochberg corrected P value (calculated as previously described)[4] of <0.05 in one biological replicate and <0.10 in the other.
2. Both melting point differences were either positive or negative in the two biological replicates.
3. The smallest absolute melting point difference of the protein in the two biological replicates was greater than the absolute melting point difference of that same protein between the two vehicle experiments.

Analysis of TPP CCR experiments. Calculation of pEC_{50} values from thermal profiling experiments over a range of compound concentrations was performed as previously described[4,13]. The vehicle condition was used as the reference for fold-change calculations for the nine compound concentrations and vehicle condition. Prior to fitting a sigmoidal dose-response curve (top and bottom fixed at 1 and 0, variable slope), the tenfold change values were transformed to a range between 0 and 1 for stabilized proteins and 1 and 0 for destabilized proteins[4,13]. We required proteins to be stabilized or destabilized by the compound treatment at the maximum concentration by at least 50% (untransformed fold changes) compared to the vehicle condition and the R^2 of the fit of the sigmoidal dose-response curve had to be >0.8 (refs. 4,13). These criteria had to be fulfilled in both biological replicates. Proteins had to be identified by at least two unique peptides in both experiments. Proteins passing these requirements were considered as affected in their thermal stability in a dose-responsive manner with the calculated pEC_{50} values.

Analysis of 2D-TPP experiments. For each of the six TMT10 experiments, we used the two vehicle conditions at the two temperatures as the reference for fold-change calculations for the two sets of four compound concentrations and vehicle condition at the respective temperatures. Proteins had to be identified by two unique peptides and quantified with reporter ions stemming from at least three distinct spectra. Before fitting sigmoidal dose-response curves for each temperature condition (with top and bottom fixed at 1 and 0, variable slope), the fivefold change values in each temperature condition were transformed to a range between 0 and 1 for stabilized proteins and 1 and 0 for destabilized proteins[4,13]. Proteins were required to be stabilized or destabilized by the compound treatment at the maximum concentration by at least 50% (untransformed fold changes) compared to the vehicle condition, and the R^2 of the fit of the sigmoidal dose-response curve had to be above 0.8 (refs. 4,13). These criteria had to be fulfilled in at least two adjacent temperature conditions in which the proteins had to be identified by at least two unique peptides. The pEC_{50} that was measured at the temperature closest to the melting point of the protein was taken as the proxy for the compound potency. If no melting point data were available for the protein, the pEC_{50} measured at the lowest temperature was used. Proteins that were either stabilized or destabilized across all temperature conditions after compound treatment were not considered for further analysis, as they were deemed to be affected in either expression or extractability, rather than thermal stability.

Metabolomics experiments. HepG2 and SH-SY5Y cells were cultured in 6-well plates as described above; all samples were generated in triplicate. Cells were treated with either vehicle (DMSO) or panobinostat (2 μM) for 4, 8 or 24 h hours. Samples of culture medium were taken from wells without cells as well as from vehicle- and panobinostat-treated cells after 8 and 24 h. Cell samples were taken by aspirating cell medium and adding lysis buffer (40% acetonitrile, 40% methanol, 20% water). Cells were scraped, transferred to tubes, incubated for 10 min at 4 °C and subjected to centrifugation (15 min, 4 °C, 20,000 × g). Supernatant was snap frozen and shipped to Biomolecular Mass Spectrometry and Proteomics, Utrecht University, for analysis.

Metabolomics analysis. LC-MS analysis was performed on an Exactive mass spectrometer (Thermo Scientific) coupled to a Dionex UltiMate 3000 autosampler and pump (Thermo Scientific). The MS operated in polarity-switching mode with spray voltages of 4.5 kV and −3.5 kV. Metabolites were separated using a Sequant ZIC-pHILIC column (2.1 × 150 mm, 5 μm, guard column 2.1 × 20 mm, 5 μm; Merck) using a linear gradient of acetonitrile and eluent A (20 mM $(NH_4)_2CO_3$, 0.1% NH_4OH in ULC/MS-grade water (Biosolve)). Flow rate was set at 150 μl/min. Essential amino acids and tyrosine were identified and quantified using LCquan software (Thermo Scientific) on the basis of exact mass within 5 p.p.m. and further validated by concordance with retention times of amino acid standards.

Normalization procedure. We used essential amino acids for normalization of cell sample data as follows, with three replicates for each time point (4, 8 and 24 h) and sample group: (i) peak intensities of each time point and compound for all essential amino acids and replicates were summed; (ii) the median of all replicates for each time point was calculated and (iii) sum peak intensity was divided by median for each data point resulting in a normalization factor for each data point to be applied on each individual amino acid peak-intensity measurement.

Inhibition of rat phenylalanine hydroxylase by panobinostat. Recombinant rat phenylalanine hydroxylase was purified from *E. coli* as described by Roberts *et al.*[29]. Recombinant rat tyrosine hydroxylase was purified from *E. coli* as described by Daubner *et al.*[30]. Tetrahydrobiopterin was purchased from Schircks Laboratories. All other major chemicals and media were

doi:10.1038/nchembio.2185

purchased from Sigma-Aldrich or Thermo Fisher Scientific and were of the highest purity commercially available. Initial rate data were fit to the inhibition equation using the program KaleidaGraph (Synergy Software).

The assay for phenylalanine hydroxylase was based on the method of Zhang *et al.*[31]. Phenylalanine hydroxylase (1.25 μM) was incubated with 1 mM phenylalanine in 0.2 M HEPES, pH 7.0, at 25 °C for 3 min to activate the enzyme. 35 μL enzyme–phenylalanine mixture was then added to 205 μL assay mix containing 0–64 μM panobinostat, 4% dimethylsulfoxide, 60 μg/mL catalase, 1 mM dithiothreitol, 5 μM ferrous ammonium sulfate, and 80 mM HEPES, pH 7.0 (concentrations after mixing). Reactions were initiated by the addition of 10 μL 625 μM tetrahydrobiopterin (final concentration 25 μM). Duplicate reactions were quenched by adding 125 μL 2 M HCl after 30 or 60 s, and the rate of tyrosine formation was determined from each to verify that the reaction was linear over this time period. The assay for DOPA production by tyrosine hydroxylase was similar. Tyrosine hydroxylase (10 μL 1.25 μM) was added to 230 μL assay mix to yield 0–64 μM inhibitor, 25 μM tyrosine, 4% dimethylsulfoxide, 60 μg mL^{-1} catalase, 1 mM dithiothreitol, 5 μM ferrous ammonium sulfate and 80 mM HEPES, pH 7.0. Assays were initiated by the addition of 10 μL 625 μM tetrahydrobiopterin and quenched with 2 M HCl after 30 and again after 60 s. For both enzymes, acid-quenched samples were centrifuged for 5 min at 10,000 × *g* to remove denatured protein. The supernatants were diluted tenfold with 0.1% acetic acid and injected onto a Gemini-NX C18 HPLC column (150 mm × 2.0 mm) with a mobile phase of 0.1% acetic acid. Tyrosine and DOPA were detected by fluorescence with the excitation wavelength set at 275 nm and the emission wavelength set at 303 nm. A standard curve of 0–100 μM L-tyrosine or 0–25 μM L-DOPA was used to quantify the amount of tyrosine or DOPA produced.

The effect of panobinostat on the activity of phenylalanine hydroxylase was determined as a function of the concentration of panobinostat. Panobinostat was either incubated with the activated enzyme for 5 min or added at the start of the assays. Identical analyses were performed with tyrosine hydroxylase.

To test whether panobinostat binds to the inactive phenylalanine hydroxylase enzyme, we added panobinostat to the preactivation mix at different concentrations, then added this mix to the incubation mix containing the same concentration of inhibitor and all other assay components.

24. Dittmann, A., Ghidelli-Disse, S., Hopf, C. & Bantscheff, M. *Methods Mol. Biol.* **1156**, 279–291 (2014).
25. Becher, I. *et al. ACS Chem. Biol.* **8**, 599–607 (2013).
26. Drewes, G. *et al.* US patent 20090238808 (2009).
27. Savitski, M.M. *et al. J. Am. Soc. Mass Spectrom.* **21**, 1668–1679 (2010).
28. Savitski, M.M. *et al. J. Proteome Res.* **12**, 3586–3598 (2013).
29. Roberts, K.M., Khan, C.A., Hinck, C.S. & Fitzpatrick, P.F. *Biochemistry* **53**, 7846–7853 (2014).
30. Daubner, S.C. & Fitzpatrick, P.F. *Biochemistry* **38**, 4448–4454 (1999).
31. Zhang, S., Hinck, A.P. & Fitzpatrick, P.F. *Biochemistry* **54**, 5167–5174 (2015).